Available online at www.sciencedirect.com

ScienceDirect

IFAC PapersOnline CONFERENCE PAPER ARCHIVE

IFAC PapersOnLine 54-20 (2021) 455–462

Developing Equations of Motion for a Planar Biped Walker with Nonuniform Foot Shape

Claire H. Rodman* Anne E. Martin*

**Pennsylvania State University, University Park, PA 16801 USA (e-mail: chr33@psu.edu)*

Abstract: Foot shape can strongly influence performance and efficiency in bipedal gait, playing a critical role in both human and robot walking. While flat feet and circular feet are common in human models, a more general shape may better capture the effective foot shape of humans, leading to an improved simulation-experimental match. The key challenge in modeling a biped with a nonuniform foot shape is locating the ankle as the foot rolls forward so that the equations of motion can be derived. This work develops a method to find the equations of motion for a planar biped whose foot shape can be modeled as any convex, continuously differentiable function. The method is demonstrated using a six-link, planar biped model with nonuniform, curved feet. Using nonlinear constrained optimization, valid gaits were identified for foot shapes parameterized by circular, elliptical, and polynomial functions. The resulting gaits were compared to experimental spatiotemporal and kinematic walking data from one human subject. The polynomial model both best approximated the subject's foot shape and best matched the experimental spatiotemporal behavior and stance ankle angle trajectory, confirming the viability of the method for both simulating gait and matching human walking.

Keywords: Dynamics and control, modeling of human performance, bipedal gait, constrained optimization

1. INTRODUCTION

Foot shape plays a significant role in the mechanics of bipedal walking (Hansen, Childress and Knox, 2004; Adamczyk, Collins and Kuo, 2006; Adamczyk and Kuo, 2013; Croft and Bertram, 2020; Schmitthenner *et al.*, 2020). The human foot is composed of several distinct segments and joints, which collectively deform as a person progresses through the gait cycle (Carson *et al.*, 2001). Studies investigating foot shape have shown that foot shape and length can reduce the work to redirect the biped center of mass when transitioning between steps (Adamczyk, Collins and Kuo, 2006; Adamczyk and Kuo, 2013), which is a significant contributor to the energetic cost of transport (Donelan, Kram and Kuo, 2002). Additionally, foot shape is a critical parameter in designing stable and efficient biped robots (Collins, Wisse and Ruina, 2001; Collins and Ruina, 2005; Martin, Post and Schmiedeler, 2014). Thus, investigating complex foot shape in gait models has implications in both the biomechanics of human walking and the performance of biped robots.

Gait models often reduce the complex anatomical degrees of freedom by representing the foot as a flat, rigid plate (Goswami, 1999; Tlalolini, Chevallereau and Aoustin, 2009). This approach is simpler than using multisegmented (Mummolo, Akbas and Carbone, 2021) or compliant (Yazdi-Mirmokhalesouni *et al.*, 2018) models, but requires additional modelling phases such as heel strike at the beginning of the step, a mid-stance transfer of support from heel to toe, and toe off at the end of the step. An alternative method is to model the foot as a circular arc that rolls without slipping in the sagittal plane (Kuo, 2001, 2007; Martin and Schmiedeler, 2014; Martin, Post and Schmiedeler, 2014; Trkov, Chen and Yi, 2019). This approach reduces the number of modelling phases and in some cases improves efficiency over flat foot models (Asano and Luo, 2006; Kwan and Hubbard, 2007). Control is relatively straightforward since the hybrid zero dynamics (HZD) based control strategy (Westervelt *et al.*, 2007) has been extended to planar biped models with circular feet (Martin, Post and Schmiedeler, 2014). This method has successfully been used with a six-link planar biped to match and predict human walking kinematics (Martin and Schmiedeler, 2014). But the model foot and ankle did not sufficiently capture the physiological complexity of the human foot and ankle, resulting in relatively low correlations between simulated and experimental ankle kinematics.

A model with nonuniform foot curvature likely could better capture the foot and ankle behavior when mimicking human walking, but it introduces new modelling challenges when deriving the equations of motion and impact map. Analytical expressions for ankle position and velocity are required for these derivations. When using a circular stance foot, the constant-height center of curvature provides a suitable reference point to locate the ankle, but for nonuniform foot shape, this point varies, complicating the necessary calculations. Some works have derived models for elliptical (Smyrli *et al.*, 2019) or piecewise (Yamane and Trutoiu, 2009) foot shapes, but these derivations were specific to the chosen foot parameterizations and are not generalizable to others. This paper provides a derivation for finding the ankle position and velocity for any foot shape that can be represented by a convex and continuously differentiable function. Concurrently, Smyrli

10.1016/j.ifacol.2021.11.215

and Papadopoulos (2020) have independently developed a similar method for locating the ankle position and carrying out the subsequent derivations when the foot shape is described using a lookup table. They illustrate their method using a passive spring-loaded inverted pendulum model with one foot shape. In contrast, this paper uses a six-link, actuated biped model to demonstrate successful walking for three representative foot shapes.

HZD control was chosen for this model due to its successful use in underactuated point- and curved-foot biped simulation (Chevallereau and Aoustin, 2001; Westervelt *et al.*, 2007; Ames, Cousineau and Powell, 2012; Chevallereau *et al.*, 2013; Martin and Schmiedeler, 2014; Martin, Post and Schmiedeler, 2014). In this method, feedback linearization drives the actuated joint angles along the desired trajectories during the single support phase (Isidori, 1989; Westervelt *et al.*, 2007). At the end of the step, the impact of the swing foot marks an instantaneous double support phase. Foot shape influences the system behavior during both phases of this hybrid model (Martin, Post and Schmiedeler, 2014).

This work derives a hybrid model for simulating a planar biped with nonuniform curved feet. The model is validated for three representative foot shapes by determining the desired gait trajectories to generate stable walking and match experimental kinematic data from a human subject. Section 2 contains the derivation of the equations of motion and impact map and a description of the controller. Section 3 describes the experimental data collection and processing and the gait matching simulation protocol. The simulation results and discussion are found in Section 4.

2. MODEL DEVELOPMENT

The planar biped model is comprised of N links connected by $N-1$ revolute joints (Martin and Schmiedeler, 2014). For illustration purposes, this work will consider a six-link model that has two thighs, two shanks, and two feet, each of which has mass and rotational inertia (Fig. 1). A point mass at the hip represents the head, arms, and torso of a person, but the rotational inertia of these segments is neglected. The feet have nonuniform curvature, which will be described further in the following sections. They roll without slipping relative to the ground, and thus the system has one degree of underactuation. The stance thigh orientation, q_1, is the unactuated generalized coordinate, and the relative joint angles, $q_2 \dots q_6$, are actuated with ideal actuators.

The hybrid model of a step consists of two alternating phases (Westervelt *et al.*, 2007). In the single support phase, the stance leg supports the biped as the swing leg moves forward. The double support phase occurs instantaneously when the swing leg impacts the ground and the stance and swing leg roles swap. Single support is modelled with continuous nonlinear differential equations, and double support is modelled using an algebraic impact map.

This section contains the derivation of this hybrid model for a biped with nonuniformly curved feet. Section 2.1 contains the parameterization of the foot shape and calculation of the ankle position and velocity. Sections 2.2 and 2.3 derive the equations of motion for single and double support, respectively by showing the effect of nonuniform curved feet on the calculation. Finally, Section 2.4 contains a description of the HZD control strategy used.

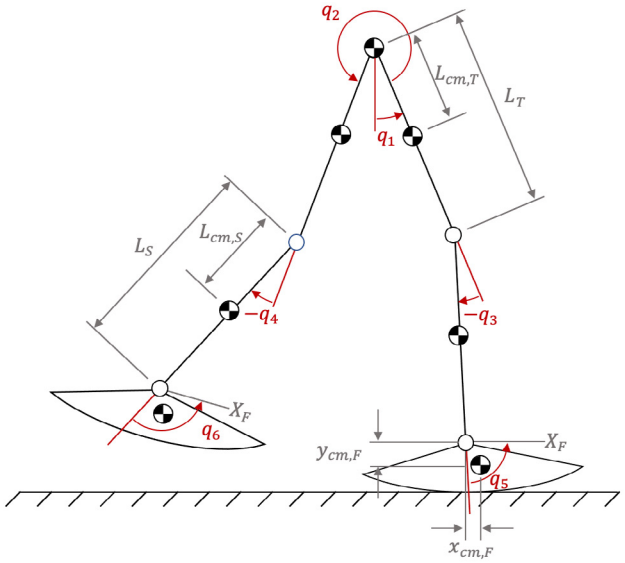

Fig. 1. Depiction of a six-link planar biped configuration during single support. Joint angles q_2, q_3, q_4, q_5, and q_6 are actuated and q_1 is unactuated. Joint positions and link COM positions are shown, measured in body-fixed reference frames from the proximal joint. Ankle angles q_5 and q_6 are measured from the shank to the foot-fixed horizontal axis X_F.

2.1 Ankle Position and Velocity

During single support, the nonlinear equations of motion have the form

$$\boldsymbol{D}(\boldsymbol{q})\ddot{\boldsymbol{q}} + \boldsymbol{C}(\boldsymbol{q},\dot{\boldsymbol{q}})\dot{\boldsymbol{q}} + \boldsymbol{G}(\boldsymbol{q}) = \boldsymbol{B}\boldsymbol{u} \tag{1}$$

where $\boldsymbol{q}$ is the $N \times 1$ vector of generalized coordinates, $\boldsymbol{u}$ is the $N-1 \times 1$ vector of joint torques, $\boldsymbol{D}$ is the $N \times N$ inertia matrix, $\boldsymbol{C}$ is the $N \times N$ Coriolis matrix, $\boldsymbol{G}$ is the $N \times 1$ gravitational vector, and $\boldsymbol{B}$ is the $N \times N-1$ matrix that converts the control inputs to joint torques. $\boldsymbol{D}, \boldsymbol{C}$, and $\boldsymbol{G}$ are derived using the Euler-Lagrange equation and thus are affected by the curvature of the foot. Finding the matrices requires the global positions and velocities of the COM of the links. These positions are calculated by working up the kinematic chain from the ground contact point C and differentiating to get the velocities. Thus, the foot must be parameterized such that the global stance ankle coordinates can be calculated for a given state of the biped.

When parameterizing the foot roll-over shape of the biped, two critical assumptions were made:

F1. The stance foot rolls along the ground without slipping, and

F2. The function describing the foot must be convex and thrice continuously differentiable for the defined range.

The following derivations are generalizable to any system that satisfies assumptions F1 and F2. Thus, the foot shape is

defined by the curve

$$ {}^{A}y_F = f_F({}^{A}x_F) \tag{2}$$

where $({}^{A}x_F, {}^{A}y_F)$ are the cartesian coordinates of the foot in an ankle-fixed reference frame. The preceding superscript and following subscript notation denote the reference frame and point, respectively. f_F is a function satisfying assumption F2 (Fig. 2a). Each point along the curve has a defined slope in ankle-fixed coordinates

$$ \frac{d\,{}^{A}y_F}{d\,{}^{A}x_F} = g_F({}^{A}x_F) \tag{3}$$

where $g_F({}^{A}x_F)$ is the derivative of $f_F({}^{A}x_F)$, relabelled for convenience later. The absolute stance foot orientation, β, is measured from the horizontal global axis and for this particular model, is defined as

$$ \beta(\boldsymbol{q}) = \frac{\pi}{2} - (q_1 + q_3 + q_5). \tag{4}$$

As the stance foot rotates through this absolute angle, the contact point C is defined as the tangential intersection between the foot curve and the ground (Fig. 2b). Because the foot is tangent to the ground at this point,

$$ g_F({}^{A}x_C) = \tan\beta(\boldsymbol{q}). \tag{5}$$

Because f_F is convex under assumption F2, g_F is by definition monotonically increasing. Thus, under the one-to-one mapping $g_F(\cdot)$, ${}^{A}x_C$ can be uniquely determined from the stance foot orientation using (3) and (5):

$$ {}^{A}x_C = {g_F}^{-1}[\tan\beta(\boldsymbol{q})]. \tag{6}$$

${}^{A}y_C$ follows from (2).

To locate the stance ankle in the global reference frame, $\boldsymbol{{}^{A}r_{AC}}$ is defined as the vector from point $\boldsymbol{A}$ to $\boldsymbol{C}$ in ankle-fixed coordinates with magnitude and direction

$$ \|\boldsymbol{{}^{A}r_{AC}}\| = \sqrt{{}^{A}x_C{}^2 + {}^{A}y_C{}^2} \tag{7a}$$

$$ \angle\,\boldsymbol{{}^{A}r_{AC}} = \tan^{-1}\frac{{}^{A}y_C}{{}^{A}x_C}. \tag{7b}$$

So, in global coordinates, the stance ankle position $({}^{O}x_A, {}^{O}y_A)$ is

$$ {}^{O}x_A = {}^{O}x_C - \|\boldsymbol{{}^{A}r_{AC}}\|\cos[\angle\,\boldsymbol{{}^{A}r_{AC}} - \beta(\boldsymbol{q})] \tag{8a}$$

$$ {}^{O}y_A = -\|\boldsymbol{{}^{A}r_{AC}}\|\sin[\angle\,\boldsymbol{{}^{A}r_{AC}} - \beta(\boldsymbol{q})] \tag{8b}$$

where ${}^{O}x_c$ is the global x-coordinate of the contact point (Fig. 2b). Under assumption F1, this point is defined as the arc length

$$ {}^{O}x_c = \int_{{}^{A}x_{C0}}^{{}^{A}x_C} \sqrt{1 + {g_F}^2({}^{A}x_F)}\; d\,{}^{A}x_F \tag{9}$$

where ${}^{A}x_{C0} = {g_F}^{-1}(0)$, as per (6) when $\beta(\boldsymbol{q}) = 0$.

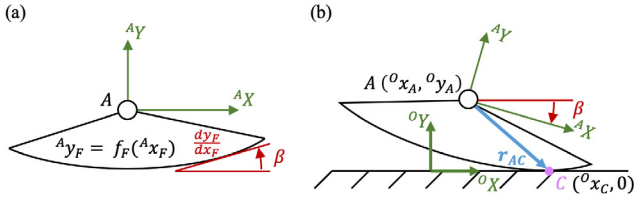

Fig. 2. Model of the foot for a general nonuniform curve. (a) The curve of the foot is described by the function f_F in an ankle-fixed reference frame with the origin at the ankle joint A. (b) The foot at an absolute orientation β in contact with the ground at point C. The foot shape curve is tangent to the ground at C, relating the ankle-fixed function slope to the foot orientation. Vector $\boldsymbol{{}^{A}r_{AC}}$ locates the contact point C relative to the ankle A.

While $g_F(\cdot)$ is inherently a one-to-one mapping, it is not necessarily analytically invertible. Thus, an indirect method for determining ${}^{A}\dot{x}_C$, ${}^{A}\dot{y}_C$, and ${}^{O}\dot{x}_C$ is required to calculate the link COM velocities. Solving (5) for β, differentiating with respect to time, and rearranging yields

$$ {}^{A}\dot{x}_C = \frac{[1+{g_F}^2({}^{A}x_C)]}{{g_F}'({}^{A}x_C)}\frac{d\beta(\boldsymbol{q})}{d\boldsymbol{q}}\,\dot{\boldsymbol{q}} \tag{10}$$

where the dot and prime denote the derivatives with respect to time and ${}^{A}x_F$, respectively. Differentiating (2) yields

$$ {}^{A}\dot{y}_C = g_F({}^{A}x_C)\,{}^{A}\dot{x}_C \tag{11}$$

and differentiating (9) using the chain rule yields

$$ {}^{O}\dot{x}_C = \frac{d\,{}^{O}x_C}{d\,{}^{A}x_C}\,{}^{A}\dot{x}_C = \sqrt{1 + {g_F}^2({}^{A}x_C)}\;{}^{A}\dot{x}_C. \tag{12}$$

Thus, substituting ${}^{A}\dot{x}_C$ from (10) into (11) and (12) yields ${}^{A}\dot{y}_C$ and ${}^{O}\dot{x}_C$ in terms of the biped states $\boldsymbol{q}$ and $\dot{\boldsymbol{q}}$. These expressions are plugged into the derivatives of (8), which are used to determine the link COM velocities.

2.2 Single Support

Once the link COM positions and velocities have been determined, the Lagrangian is determined as $L = K - V$, where K and V are the kinetic and potential energy of the system. The Euler-Lagrange method is applied, yielding $\boldsymbol{D}$ directly, as the terms of K are linear with respect to $\dot{\boldsymbol{q}}$. Calculating $\boldsymbol{G}$ and $\boldsymbol{C}$, however, involves differentiating with respect to $\boldsymbol{q}$. $\boldsymbol{G}$ is calculated as

$$ \boldsymbol{G} = \frac{dV}{d\boldsymbol{q}} \tag{13}$$

and $\boldsymbol{C}$ is formulated from (Spong and Vidyasagar, 1989):

$$ C_{jk} = \sum_{i=1}^{6} \frac{1}{2}\left[\frac{\partial D_{kj}}{\partial q_i} + \frac{\partial D_{ki}}{\partial q_j} - \frac{\partial D_{ij}}{\partial q_k}\right]\dot{q}_i \tag{14}$$

where k, j denote rows and columns of $\boldsymbol{C}$. The elements of V and $\boldsymbol{D}$ are expressed in terms of ${}^{A}x_C$ and ${}^{A}y_C$. Because these terms do not necessarily have analytically separable expressions in terms of $\boldsymbol{q}$, the chain rule must be employed to complete the partial derivatives of V and $\boldsymbol{D}$ with respect to $\boldsymbol{q}$.

This calculation requires analytical expressions for $\frac{d\,{}^{A}x_C}{dq}$ and $\frac{d\,{}^{A}y_C}{dq}$. Following the same procedure to get (10) and (11) but differentiating with respect to $\boldsymbol{q}$ instead of time yields

$$\frac{d\,{}^{A}x_C}{d\boldsymbol{q}} = \frac{[1+{g_F}'^2({}^{A}x_C)]}{{g_F}'({}^{A}x_C)}\frac{d\beta(\boldsymbol{q})}{d\boldsymbol{q}} \tag{15}$$

$$\frac{d\,{}^{A}y_C}{d\boldsymbol{q}} = {g_F}'({}^{A}x_C)\frac{d\,{}^{A}x_C}{d\boldsymbol{q}}. \tag{16}$$

$\boldsymbol{B}$ is unaffected by the foot shape. Thus, the equations of motion for a biped with any foot shape described by function f_F that satisfies assumptions F1 and F2 can be found using (15) and (16) along with standard Euler-Lagrange methods.

2.3 Instantaneous Double Support

At the end of the single support phase, the swing leg impacts the ground, marking the end of the previous step and resetting the leg roles for the beginning the next one. This impact is modelled as an instantaneous inelastic collision, with the impacting foot rolling without slipping and the back foot lifting without interaction from the ground (Martin, Post and Schmiedeler, 2014). Because the impact is instantaneous, the biped configuration is assumed constant during the event. An algebraic impact map determines the joint angles and velocities just after the impact based on those just prior. Because the biped model is one-step symmetric, the impact map also swaps the stance and swing leg roles so that the same equations of motion can simulate steps with both the left and right leg in stance. This mapping takes the form

$$\boldsymbol{q}^+ = \boldsymbol{S}\boldsymbol{q}^- \tag{17a}$$

$$\dot{\boldsymbol{q}}^+ = \boldsymbol{A}(\boldsymbol{q}^-)\dot{\boldsymbol{q}}^- \tag{17b}$$

where $\boldsymbol{q}^-$and $\boldsymbol{q}^+$ are the biped configuration immediately pre- and post-impact, $\boldsymbol{S}$ is an $N \times N$ matrix that swaps the stance and swing leg roles, and $\boldsymbol{A}$ is an $N \times N$ matrix that maps the joint velocities. Similar to the single support matrices, $\boldsymbol{A}$ is affected by foot curvature (Martin, Post and Schmiedeler, 2014).

Calculating $\boldsymbol{A}$ requires the reaction forces at the feet, so the extended equations of motion with a Lagrange multiplier term are determined using the Euler-Lagrange approach. Using extended generalized coordinates, $\boldsymbol{q_e} = [\boldsymbol{q}^T, {}^{O}x_H, {}^{O}y_H]^T$ where $({}^{O}x_H, {}^{O}y_H)$ are the global coordinates of the hip, the extended equations of motion are integrated, resulting in a set of $N+2$ equations describing the conservation of momentum at impact. This integration assumes that the impact force is impulsive and thus the resulting ground reaction forces are significantly higher than those due to gravity or the actuators in this instant. To solve for the post-impact extended generalized coordinate velocities and the impulsive impact forces ($N+4$ unknowns), two additional equations are required. These equations are represented by

$$\boldsymbol{E}(\boldsymbol{q_e^-})\dot{\boldsymbol{q}}_{\boldsymbol{e}}^+ = 0 \tag{18}$$

where $\boldsymbol{E}$ is a $2 \times N+2$ matrix and the Jacobian of the constraint equations, which enforce the no-slip and lifting-without-interaction conditions. The constraint matrix $\boldsymbol{E}$ is determined by differentiating a vector loop with respect to $\boldsymbol{q_e}$:

$${}^{O}\boldsymbol{r_{0H}} + {}^{O}\boldsymbol{r_{HF}} + {}^{O}\boldsymbol{r_{F0}} = \boldsymbol{0} \tag{19}$$

where ${}^{O}\boldsymbol{r_{0H}}$, ${}^{O}\boldsymbol{r_{HF}}$, and ${}^{O}\boldsymbol{r_{F0}}$ are the vectors from the global reference frame origin to the hip, from the hip to the contact point of the impacting foot, and from the contact point of the impacting foot to the global origin in terms of $\boldsymbol{q_e}$. Differentiating (19) yields

$$E = \frac{d\,{}^{O}\boldsymbol{r_{0H}}}{d\boldsymbol{q_e}} + \frac{d\,{}^{O}\boldsymbol{r_{HF}}}{d\boldsymbol{q_e}} + \frac{d\,{}^{O}\boldsymbol{r_{F0}}}{d\boldsymbol{q_e}} \tag{20a}$$

where

$$\frac{d\,{}^{O}\boldsymbol{r_{0H}}}{d\boldsymbol{q}} = [\boldsymbol{0}_{2\times N} \quad \boldsymbol{I}_{2\times 2}] \tag{20b}$$

$$\frac{d\,{}^{O}\boldsymbol{r_{HF}}}{d\boldsymbol{q}} = \left[\frac{\partial\,{}^{O}\boldsymbol{r_{HF}}}{\partial\boldsymbol{q}} + \frac{\partial\,{}^{O}\boldsymbol{r_{HF}}}{\partial\,{}^{A}x_C}\frac{\partial\,{}^{A}x_C}{\partial\boldsymbol{q}} + \frac{\partial\,{}^{O}\boldsymbol{r_{HF}}}{\partial\,{}^{A}y_C}\frac{\partial\,{}^{A}y_C}{\partial\boldsymbol{q}} \quad \boldsymbol{0}_{2\times 2}\right] \tag{20c}$$

$$\frac{d\,{}^{O}\boldsymbol{r_{F0}}}{d\boldsymbol{q}} = \begin{bmatrix} -\frac{d\,{}^{O}x_{C,im}}{d\boldsymbol{q}} & \boldsymbol{0}_{2\times 2} \\ \boldsymbol{0}_{1\times N} & \end{bmatrix} \tag{20d}$$

and $\frac{d\,{}^{O}x_{C,im}}{d\boldsymbol{q}}$ is the derivative of the impacting foot contact point with respect to $\boldsymbol{q}$. Using the chain rule on (9) yields

$$\frac{d\,{}^{O}x_{C,im}}{d\boldsymbol{q}} = \frac{d\,{}^{O}x_C}{d\,{}^{A}x_C}\frac{d\,{}^{A}x_C}{d\boldsymbol{q}} = \sqrt{1+{g_F}^2({}^{A}x_C)}\frac{d\,{}^{A}x_C}{d\boldsymbol{q}}. \tag{20e}$$

Finally, solving the extended conservation of momentum equations and constraint equations for $\dot{\boldsymbol{q}}^+$ in terms of $\dot{\boldsymbol{q}}^-$ yields $\boldsymbol{A}$. This completes the parameterization of the hybrid model for a planar biped with nonuniform curved feet.

2.4 Control

This work uses HZD-based control, as shown in Martin, Post and Schmiedeler (2014). The non-uniform foot shape does not directly affect the controller, so only a brief derivation is included here for completeness. The equations of motion in (1) can be expressed as a first order system of the form

$$\dot{\boldsymbol{x}} = \begin{bmatrix} \dot{\boldsymbol{q}} \\ \boldsymbol{D}^{-1}(-\boldsymbol{C}\dot{\boldsymbol{q}} - \boldsymbol{G}) \end{bmatrix} + \begin{bmatrix} \boldsymbol{0} \\ \boldsymbol{D}^{-1}\boldsymbol{B} \end{bmatrix}\boldsymbol{u} \tag{21a}$$

$$\dot{x} = \boldsymbol{f}(\boldsymbol{x}) + \boldsymbol{g}(\boldsymbol{x})\boldsymbol{u} \tag{21b}$$

where $\boldsymbol{x} = [\boldsymbol{q}^T, \dot{\boldsymbol{q}}^T]^T$ is the state vector. The output $\boldsymbol{y} = \boldsymbol{h}(\boldsymbol{q})$ is an $N-1 \times 1$ vector of the error between the actuated joint angles and the desired trajectories. The desired joint angle trajectories are represented as fifth order Bezier polynomials. Differentiating $\boldsymbol{y}$ twice yields

$$\ddot{\boldsymbol{y}} = L_{\boldsymbol{f}}^2\boldsymbol{h} + L_{\boldsymbol{g}}L_{\boldsymbol{f}}\boldsymbol{h}\,\boldsymbol{u} \tag{22}$$

where $L_{\boldsymbol{f}}^2\boldsymbol{h}$ and $L_{\boldsymbol{g}}L_{\boldsymbol{f}}\boldsymbol{h}$ are Lie derivatives (Isidori, 1989). Performing input-output linearization gives

$$\boldsymbol{u} = L_f L_{\boldsymbol{g}}\boldsymbol{h}^{-1}\left(\boldsymbol{v} - L_{\boldsymbol{f}}^2\boldsymbol{h}\right) \tag{23}$$

Table 1. Model parameters. The legs are symmetric, so the values are the same for both.

Parameter	Value	Description
Thighs		
L_T	0.394	Thigh length (m)
$L_{cm,T}$	0.171	Thigh COM position (m)
m_T	6.07	Thigh mass (kg)
J_T	0.099	Thigh Moment of Inertia (kg.m^2)
Shanks		
L_S	0.396	Shank length (m)
$L_{cm,S}$	0.172	Shank COM position (m)
m_S	2.82	Shank mass (kg)
J_S	0.040	Shank Moment of Inertia (kg.m^2)
Feet		
$x_{cm.F}$	0.046	Foot horizontal COM position (m)
$y_{cm,F}$	0.122	Foot vertical COM position (m)
m_F	0.880	Foot mass (kg)
J_T	0.012	Foot Moment of Inertia (kg.m^2)
Body		
m_{HAT}	41.2	Head, arms, and torso mass (kg)
Control		
k_P	1000	Proportional gain
k_D	100	Derivative gain

where $\boldsymbol{v} = -k_P\boldsymbol{y} - k_D\dot{\boldsymbol{y}}$ with feedback gains k_P and k_D chosen to drive the output to zero even in the presence of disturbances.

3. MODEL VALIDATION

To validate the model derived above, simulated gait trajectories modelled using three different foot shapes were compared to the experimental kinematics for one human subject. Section 3.1 describes the experimental methods used to collect and process the walking data. Section 3.2 describes the simulation procedure for generating representative viable gaits for the three foot shapes explored.

3.1 Experimental Methods

After obtaining informed consent, one subject (height 1.74 m, weight 61.2 kg) walked on an instrumented, split-belt treadmill (Bertec, Columbus, OH) at a constant speed of 1.07 m/s for one minute. The embedded force plates measured ground reaction forces and center of pressure (COP). Joint kinematics of the legs were recorded with a Vicon Vero camera system.

The ground reaction force data were used to detect heel strike and toe off events. Because the experimental gait has a finite time double support period in contrast with the instantaneous phase of the model, the transition between steps was chosen as halfway between the double support heel strike and toe off events. Step time was normalized between 0 (beginning of the step) and 1 (end of the step). The sagittal plane COP and hip, knee, and ankle joint angles were delimited by step, and the mean and standard deviation were calculated. Step length and step time were also calculated.

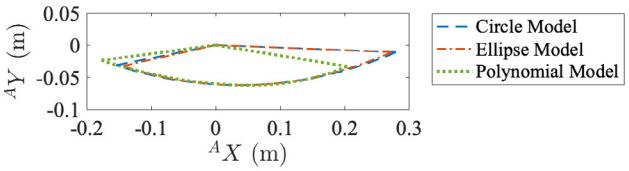

Fig. 3. The circle, ellipse, and polynomial foot shape models for one subject. Each function is plotted for the stance foot orientation range -18.4 ≤ β ≤ 23.7 degrees.

3.2 Simulation Methods

The key purpose of the simulation testing was to ensure that the biped was able to walk with a range of nonuniform foot shapes. A secondary goal was to begin determining which foot shape allowed the model to best mimic human walking. Thus, the model was scaled according to the subject's height and mass using standard anthropometric proportions from Winter (2009). The specific model parameters used are shown in Table 1. To ascertain the subject's foot shape, the COP data was transformed into a foot-fixed reference frame with the ankle at the origin (Hansen, Childress and Knox, 2004). Using least-squares curve fitting, three foot shape functions were fit to the data: a circle

$$f_{F,C}({}^A x_F) = {}^A y_{F0,C} - \sqrt{R^2 - \left({}^A x_F - {}^A x_{F0,C}\right)^2} \quad (23a)$$

where R is the radius and $({}^A x_{F0,C}, {}^A y_{F0,C})$ is the offset of the circle center relative to the ankle; an ellipse

$$f_{F,E}({}^A x_F) = {}^A y_{F0,E} - \sqrt{b^2 - \frac{b^2}{a^2}\left({}^A x_F - {}^A x_{F0,E}\right)^2} \quad (23b)$$

where a, b are the major and minor axes and $({}^A x_{F0,E}, {}^A y_{F0,E})$ is the offset of the ellipse center relative to the ankle; and a fourth-order polynomial

$$f_{F,P}\left({}^A x_F\right) = a_4\,{}^A x_F^4 + a_3\,{}^A x_F^3 + a_2\,{}^A x_F^2 + a_1\,{}^A x_F + a_0 \quad (23c)$$

where $\{a_0, a_1, a_2, a_3, a_4\}$ is a set of coefficients that satisfy the convexity requirement of F2. Other convex functions are possible, but these functions described the data well. The functions are constrained by the maximum and minimum absolute stance foot angle observed experimentally. The three subject-specific foot shapes are shown in Fig. 3. The polynomial function fit the COP data best, followed by the ellipse and then the circle.

To simulate the scaled biped model, the actuated joint angle trajectories were parameterized using fifth-order Bezier polynomials. To find a set of Bezier coefficients describing a representative gait for a particular foot shape, nonlinear constrained optimization was used. The objective function minimized the difference between the simulated and experimental spatiotemporal parameters step time, step length, and speed. Constraints were used to ensure the gait was valid. Key constraints included periodic walking and no slipping or lifting at the foot-ground contact point. In addition, the Bezier coefficients were limited to a small region around the initial

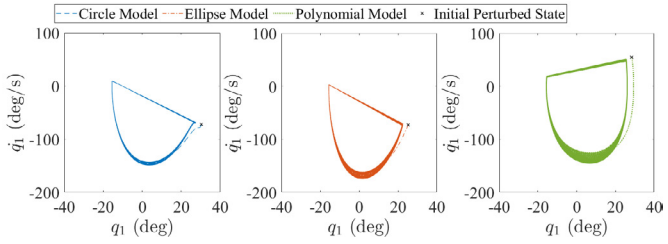

Fig. 4. Stance hip generalized coordinate phase portraits for each foot shape model. The trajectories converge to a stable limit cycle in response to a small perturbation.

conditions because the optimization tended to jump to regions where the biped could not take a step when the Bezier coefficients were not constrained. The initial optimization guess used a hand-tuned gait that could take a step using all three foot shapes, although not all constraints were met. The optimization was executed ten consecutive times for each foot shape, starting from the hand-tuned gait for the first optimization and using the result of the previous optimization as the initial condition for the subsequent optimizations. The gait corresponding to the lowest local minimum was selected.

To compare the simulated generalized coordinate trajectories to the corresponding experimental kinematics, the Pearson's correlation coefficient and root mean square error (RMSE) were determined for each joint. These values indicate how well the simulated and experimental results agree.

4. RESULTS AND DISCUSSION

4.1 Identifying Valid Gaits

Valid gaits that minimized the objective function were identified for each foot shape model. To confirm stability, the same perturbation for each model was applied to its initial post-impact state, and the model was simulated for 100 steps. The phase portrait of the resulting stance hip generalized coordinate for each model is shown in Fig. 4, confirming the presence of a stable limit cycle for all foot shape models.

4.2 Spatiotemporal Behavior

The spatiotemporal parameters for each simulated model and the experimental results are shown in Table 2. The model with circular feet best matched the experimental walking speed, but significantly underestimated the step time and step length by approximately 25%. The ellipse foot shape model severely underestimated the step time and length by approximately 40%

and 30% respectively and overestimated the speed by 17%. The polynomial foot shape model results were the best experimental match for all three parameters overall, underestimating the step time, step length, and speed by 4%, 15%, and 11%, respectively.

4.3 Kinematic Behavior

The experimental and simulated hip, knee, and ankle angle trajectories for one stride are shown in Fig. 5. The stance and swing hip angles exhibited correlation coefficients greater than

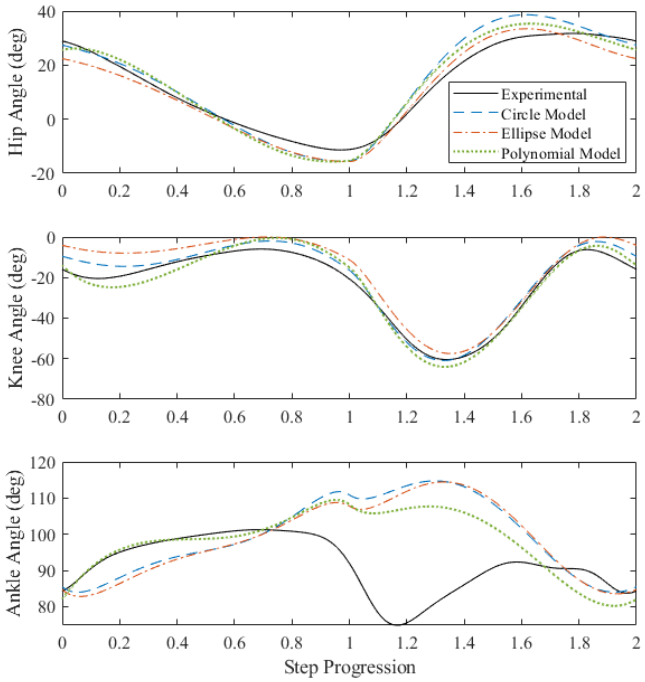

Fig. 5. Joint angle trajectories for the hip (top), knee (middle), and ankle (bottom) over one stride. When the step progression is between 0 and 1, the limb is in stance and when the step progression is between 1 and 2, the limb is in swing. The stance and swing knee and ankle joint angles correspond directly to the generalized coordinates. The hip splay, however, was transformed to absolute thigh orientation during swing to maintain continuity in this plot.

0.99 and RMSE lower than 6.1 degrees for all three foot shape models, indicating good agreement between simulated and experimental data for this joint (Tables 3 and 4). Both the simulated stance and swing knee angle trajectories also matched the experimental results well, with correlation coefficients above 0.90 and 0.99 and RMSE below 8.7 and 5.5 degrees respectively for all foot models.

The simulated stance ankle trajectories demonstrated moderate experimental agreement, with correlation coefficients of 0.60, 0.66, and 0.71 and RMSE of 6.8, 6.6, and 4.7 degrees for the circle, ellipse, and polynomial, respectively. Notably, the correlation coefficient increases and the RMSE decreases at the stance ankle joint as the foot shape function fit improves, with the polynomial foot simulation matching the experimental trajectories better than the ellipse and the circle foot model simulations. This trend indicates that improving the

Table 2. Spatiotemporal parameters for the three foot shape models and experimental data.

Model	Step Time (s)	Step Length (m)	Speed (m/s)
Circle	0.381	0.387	1.018
Ellipse	0.296	0.368	1.246
Polynomial	0.470	0.446	0.948
Experimental	0.489	0.523	1.069

Table 3. Pearson's correlation coefficients between the simulated and experimental joint trajectories for the three foot models.

Model	q_1	q_2	q_3	q_4	q_5	q_6
Circle	0.992	0.998	0.931	0.996	0.600	-0.463
Ellipse	0.993	0.997	0.917	0.991	0.657	-0.405
Polynomial	0.991	0.998	0.903	0.997	0.712	-0.465

Table 4. RMSE in degrees between the simulated and experimental joint trajectories for the three foot models.

Model	q_1	q_2	q_3	q_4	q_5	q_6
Circle	2.56	6.08	4.31	3.05	6.81	22.27
Ellipse	3.49	3.70	8.66	5.50	6.58	21.63
Polynomial	3.22	4.44	4.63	2.63	4.68	17.97

biped model by incorporating nonuniform foot shapes to better capture the effective human foot shape improves the simulation-experimental kinematic agreement of the stance ankle during human walking.

In contrast, the swing foot trajectory was negatively correlated for all foot shape models, with correlation coefficients less than -0.41. The RMSE for this joint angle trajectory was greater than 18.0 degrees for all models, more than double those of the other joints. Despite the poor simulation-experiment agreement for this joint, however, the RMSE decreased across foot shape models as the foot shape function fit improved.

These results demonstrate that the method described in Section 2 can be used to generate valid walking gaits for a six-link biped with curved feet described by both uniform and nonuniform functions. Further, the preliminary simulations suggest that using a foot shape that matches the effective human foot shape better than a circular arc improves both spatiotemporal and kinematic agreement. While some simulation-experiment discrepancies remain, both in the spatiotemporal behavior and swing ankle kinematics, additional optimization with other objective functions could likely rectify these issues. For example, Martin and Schmiedeler (2014) used an objective function that minimized the difference not only between the simulated and experimental spatiotemporal behavior but also the kinematic trajectories as well. Additionally, systematically varying the optimization initial conditions and tolerances could help identify additional local minima, as the optimization objective function appears to be highly nonlinear. Including a finite-time double support phase may also improve the simulation-experimental agreement during the step-to-step transition in the gait cycle (Williams and Martin, 2019; Williams and Martin, 2021). However, the methods used in this work successfully establish a proof of concept for simulated gait matching of human walking.

ACKNOWLEDGEMENTS

This work was supported by the National Science Foundation under Award Number 1943561 and the National Science Foundation Graduate Research Fellowship Program under Grant No. DGE1255832. Any opinions, findings, and conclusions or recommendations expressed in this material are those of the authors and do not necessarily reflect the views of the National Science Foundation.

REFERENCES

Adamczyk, P. G., Collins, S. H. and Kuo, A. D. (2006) 'The advantages of a rolling foot in human walking', *Journal of Experimental Biology*, 209(20), pp. 3953–3963. doi: 10.1242/jeb.02455.

Adamczyk, P. G. and Kuo, A. D. (2013) 'Mechanical and energetic consequences of rolling foot shape in human walking', *Journal of Experimental Biology*, 216(14), pp. 2722–2731. doi: 10.1242/jeb.082347.

Ames, A. D., Cousineau, E. A. and Powell, M. J. (2012) 'Dynamically stable bipedal robotic walking with NAO via human-inspired hybrid zero dynamics', *HSCC'12 - Proceedings of the 15th ACM International Conference on Hybrid Systems: Computation and Control*, pp. 135–144. doi: 10.1145/2185632.2185655.

Asano, F. and Luo, Z. W. (2006) 'On energy-efficient and high-speed dynamic biped locomotion with semicircular feet', *IEEE International Conference on Intelligent Robots and Systems*. IEEE, pp. 5901–5906. doi: 10.1109/IROS.2006.282470.

Carson, M. C. *et al.* (2001) 'Kinematic analysis of a multi-segment foot model for research and clinical applications: A repeatability analysis', *Journal of Biomechanics*, 34(10), pp. 1299–1307. doi: 10.1016/S0021-9290(01)00101-4.

Chevallereau, C. *et al.* (2013) 'RABBIT: A Testbed for Advanced Control Theory', *IEEE Control Systems Magazine*, 23(5), pp. 57–79.

Chevallereau, C. and Aoustin, Y. (2001) 'Optimal reference trajectories for walking and running of a biped robot', *Robotica*, 19(5), pp. 557–569. doi: 10.1017/S0263574701003307.

Collins, S. H. and Ruina, A. (2005) 'A Bipedal Walking Robot with Efficient and Human-Like Gait', *Proceedings - IEEE International Conference on Robotics and Automation*, (April), pp. 1983–1988. doi: 10.1109/ROBOT.2005.1570404.

Collins, S. H., Wisse, M. and Ruina, A. (2001) 'A Three-Dimensional Passive-Dynamic Walking Robot with Two Legs and Knees', *The International Journal of Robotics Research*, 20(7), pp. 607–615.

Croft, J. L. and Bertram, J. E. A. (2020) 'Form in the context of function: Fundamentals of an energy effective striding walk, the role of the plantigrade foot and its expected size', *American Journal of Physical Anthropology*, 173(4), pp. 760–767. doi: 10.1002/ajpa.24122.

Donelan, J. M., Kram, R. and Kuo, A. D. (2002) 'Mechanical work for step-to-step transitions is a major determinant of the metabolic cost of human walking', *Journal of Experimental Biology*, 205(23), pp. 3717–3727.

Goswami, A. (1999) 'Postural stability of biped robots and the foot-rotation indicator (FRI) point', *International Journal of Robotics Research*, 18(6), pp. 523–533. doi: 10.1177/02783649922066376.

Hansen, A. H., Childress, D. S. and Knox, E. H. (2004) 'Roll-over shapes of human locomotor systems: Effects of walking speed', *Clinical Biomechanics*, 19(4), pp. 407–414. doi: 10.1016/j.clinbiomech.2003.12.001.

Isidori, A. (1989) *Nonlinear Control Systems*. Berlin; New York: Springer-Verlag.

Kuo, A. D. (2001) 'A simple model of bipedal walking predicts the preferred speed-step length relationship', *Journal of Biomechanical Engineering*, 123(3), pp. 264–269. doi: 10.1115/1.1372322.

Kuo, A. D. (2007) 'The six determinants of gait and the inverted pendulum analogy: A dynamic walking perspective', *Human Movement Science*, 26(4), pp. 617–656. doi: 10.1016/j.humov.2007.04.003.

Kwan, M. and Hubbard, M. (2007) 'Optimal foot shape for a passive dynamic biped', *Journal of Theoretical Biology*, 248(2), pp. 331–339. doi: 10.1016/j.jtbi.2007.05.008.

Martin, A. E., Post, D. C. and Schmiedeler, J. P. (2014) 'Design and experimental implementation of a hybrid zero dynamics-based controller for planar bipeds with curved feet', *International Journal of Robotics Research*, 33(7), pp. 988–1005. doi: 10.1177/0278364914522141.

Martin, A. E. and Schmiedeler, J. P. (2014) 'Predicting human walking gaits with a simple planar model', *Journal of Biomechanics*. Elsevier, 47(6), pp. 1416–1421. doi: 10.1016/j.jbiomech.2014.01.035.

Mummolo, C., Akbas, K. and Carbone, G. (2021) 'State-Space Characterization of Balance Capabilities in Biped Systems with Segmented Feet', *Frontiers in Robotics and AI*, 8(February), pp. 1–16. doi: 10.3389/frobt.2021.613038.

Schmitthenner, D. *et al.* (2020) 'The Effect of Stiff Foot Plate Length on Walking Gait Mechanics', *Journal of Biomechanical Engineering*, 142(9), pp. 1–9. doi: 10.1115/1.4046882.

Smyrli, A. *et al.* (2019) 'On the effect of semielliptical foot shape on the energetic efficiency of passive bipedal gait', *IEEE International Conference on Intelligent Robots and Systems*, pp. 6302–6307. doi: 10.1109/IROS40897.2019.8967565.

Smyrli, A. and Papadopoulos, E. (2020) 'A methodology for the incorporation of arbitrarily-shaped feet in passive bipedal walking dynamics', *Proceedings - IEEE International Conference on Robotics and Automation*, pp. 8719–8725. doi: 10.1109/ICRA40945.2020.9196617.

Spong, M. W. and Vidyasagar, M. (1989) *Robot Dynamics and Control*. John Wiley & Sons.

Tlalolini, D., Chevallereau, C. and Aoustin, Y. (2009) 'Comparison of different gaits with rotation of the feet for a planar biped', *Robotics and Autonomous Systems*. Elsevier B.V., 57(4), pp. 371–383. doi: 10.1016/j.robot.2008.09.008.

Trkov, M., Chen, K. and Yi, J. (2019) 'Bipedal Model and Hybrid Zero Dynamics of Human Walking With Foot Slip', *Journal of Computational and Nonlinear Dynamics*, 14(10), pp. 1–12. doi: 10.1115/1.4043360.

Westervelt, E. R. *et al.* (2007) *Feedback Control of Dynamic Bipedal Robot Locomotion*. Boca Raton, FL: CRC Press.

Williams, D. S. and Martin, A. E. (2019) 'Effect of finite-time DS controllers on disturbance rejection for planar bipeds', *Proceedings of the American Control Conference*. American Automatic Control Council, pp. 4573–4579. doi: 10.23919/acc.2019.8814423.

Williams, D. S. and Martin, A. E. (2021) 'Does a finite-time double support period increase walking stability for planar bipeds?', *Journal of Mechanisms and Robotics*, 13(1), pp. 1–10. doi: 10.1115/1.4048832.

Winter, D. A. (2009) *Biomechanics and Motor Control of Human Movement*. 4th edn. Hoboken, NJ: John Wiley & Sons.

Yamane, K. and Trutoiu, L. (2009) 'Effect of foot shape on locomotion of active biped robots', *9th IEEE-RAS International Conference on Humanoid Robots, HUMANOIDS09*. IEEE, pp. 230–236. doi: 10.1109/ICHR.2009.5379576.

Yazdi-Mirmokhalesouni, S. D. *et al.* (2018) 'Modeling, control and analysis of a curved feet compliant biped with HZD approach', *Nonlinear Dynamics*. Springer Netherlands, 91(1), pp. 459–473. doi: 10.1007/s11071-017-3881-7.